# ITO-free silicon heterojunction solar cells with ZnO:Al/SiO$_2$ front electrodes reaching a conversion efficiency of 23 %

Anna B. Morales-Vilches[1], Alexandros Cruz[1], Sebastian Pingel[1], Sebastian Neubert[1], Luana Mazzarella[1], Daniel Meza[2], Lars Korte[2], Rutger Schlatmann[1], Bernd Stannowski[1]

**[1]**Helmholtz-Zentrum Berlin, PVcomB, Schwarzschildstr. 3, 12489, Berlin, Germany

**[2]**Helmholtz-Zentrum Berlin, Institut for Silicon Photovoltaics, Kekuléstr. 5, 12489, Berlin, Germany

*Abstract* — **Silicon heterojunction solar cells (SHJ) have been increasingly attracting attention to the PV community in the last years due to their high efficiency potential and the lean production process. We report on the development of a stable baseline process for SHJ cells with a focus on the optical improvement of the solar cells' front side. An amorphous silicon oxide layer (a-SiO$_2$) was used as an anti-reflective coating (AR) on top of the finished SHJ devices. Both optical simulations and experimental results demonstrate a short circuit current density (J$_{sc}$) improvement of 0.4 mA/cm$^2$ when applying the a-SiO$_2$ AR, yielding maximum conversion efficiencies of 23.0 %. Full-size cells with 244-cm$^2$ total area have been produced using three front contact stacks: ITO as reference, ZnO:Al and ZnO:Al/SiO$_2$ showing the J$_{sc}$ improvement with the double AR configuration. Damp-heat tests on those samples are currently being carried out.**

*Index Terms* — **Silicon Heterojunction Solar Cells, passivation, anti-reflective coating, aluminum-doped zinc oxide, silicon dioxide.**

## I. INTRODUCTION

Silicon heterojunction (SHJ) solar cells have been studied extensively in the past decades. Kaneka demonstrated a high power conversion efficiency potential of this technology with efficiencies of 25.1 % in a two-side contacted device (24.5 % on total area) [1] and 26.7 % in an all-rear-contacted cell design [2]. Although the highest cell efficiency was obtained in an all-rear-contacted cell design, two-side contacted cell structures are very attractive for industrialization due to their well established and lean production process. A major drawback as compared to other cell concepts is the requirement of a transparent conducting oxide (TCO) front contact for lateral carrier collection, such as indium tin oxide (ITO), and the restriction to low temperatures of approx. 200°C for metallization due to the limited temperature stability of the amorphous silicon based passivation. Both add to the manufacturing costs and might limit the cell performance optically and electrically.

We have been developing a baseline process for such two-side contacted SHJ cells over the past years. This baseline process allows to continuously develop the solar cell performance introducing innovations in all fabrication steps. Our process is based on n-type Czochralski (Cz) Si wafers with a resistivity of 5 Ωcm and DC-sputtered ITO as the front TCO. We changed from cells with an a-Si:H p-type emitter on the front side of the cell to a rear-emitter design. This design increased the short current density, J$_{sc}$, due to the more transparent and lower parasitic absorption nanocrystalline silicon n layer (nc-Si:H) used as a front surface field (FSF) compared to the amorphous silicon based (p) layer of the emitter. Moreover, this configuration allows for using less conductive TCOs due to the additional contribution of the n-type silicon wafer to lateral carrier transport [3]. Introducing optimized wet chemistry processes for random pyramid texturing, allowed a further improvement in J$_{sc}$ due to an optimized and more homogeneous pyramid size. A busbarless screen-printed silver contact grid with 12 approx. 45-µm wide fingers and an area coverage of approx. 3 % was introduced to further improve J$_{sc}$. With this SHJ *baseline processes* which were used for the present study we reach a median cell efficiency of 22.7 %, measured in-house. A cell efficiency of 22.54 % was certified by ISFH CalTeC for a 4-cm² cell using the *baseline process* described above (Fig. 1) [4]. Development of full-area cells (244-cm²) is ongoing, currently yielding a cell efficiency of 21.6 % in a bifacial busbarless layout based on the above mentioned baseline processes.

Taking benefit of the rear-emitter cell structure, we have been investigating alternative, potentially low-cost TCOs such as aluminum-doped zinc oxide (ZnO:Al). Different groups have already reported on the use of ZnO based TCOs for SHJ solar cell applications [5-7]. In this work we present results on SHJ cells that use ZnO:Al as both front and back TCOs demonstrating conversion efficiencies as high as 22.8%. Supported by optical simulations, we demonstrate an optical improvement of the SHJ finished cells when introducing an additional plasma-enhanced chemical vapor deposited (PECVD) silicon dioxide (a-SiO$_2$) antireflection (AR) layer on top of the ZnO:Al. This double AR stack concept has been used in the past by other groups using different materials (ITO, IWO as TCO and MgF$_2$ or SiO$_2$ as AR coating) showing also a clear optical improvement due to the double layer [8-15]. However, little or none of this AR benefit will remain in an encapsulated module due to the refractive index of the polymer encapsulation foil having the same value of about 1.5 as the a-SiO$_2$. Even more important for the ZnO:Al is the *protective* effect of the a-SiO$_2$ capping for the module stability as shown previously [14] and which we demonstrate in this study. Fig. 2 shows a schematic of the SHJ cell structures used in this work, i.e. monofacial rear-emitter cells with (right) and without (left) the a-SiO$_2$ AR capping layer.
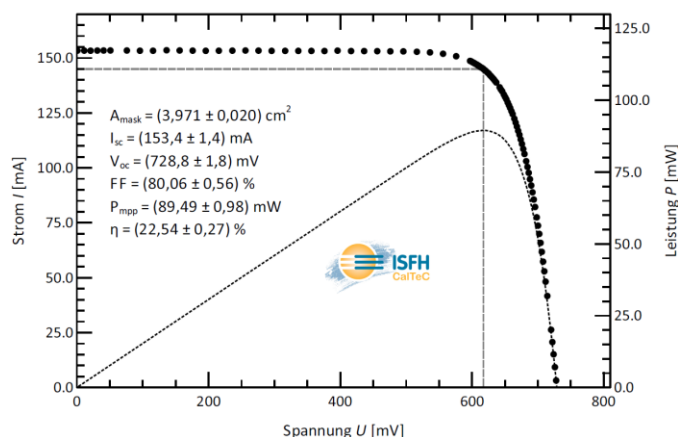
Fig. 1. Certificated I-V curve of the best HZB baseline ITO cell that uses the same PECVD layers as in the cells from this work [4], the inset shows the electrical parameters measured at ISFH CalTeC.
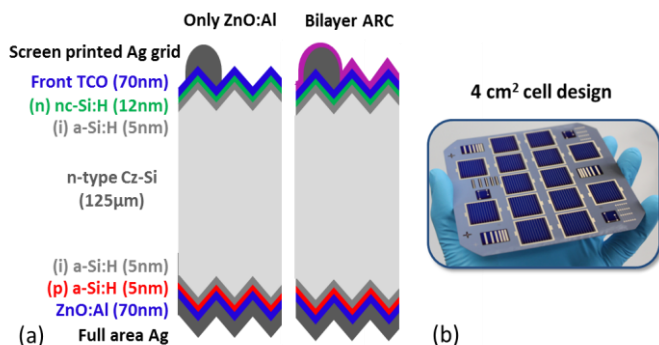


Fig. 2. (a) Schematic cross-section of the monofacial rear emitter (RE) SHJ solar cell structure fabricated in this work with aluminium-doped zinc oxide (ZnO:Al) as a single antireflection coating, left, and with the bilayer approach a-SiO$_2$/ZnO:Al, right. (b) Picture of the 4-cm$^2$ 14 cell design.

Damp-heat stability tests are being done on 244-cm$^2$ cells encapsulated as single-cell-modules using ITO as a reference, ZnO:Al, and the capped ZnO:Al/a-SiO$_2$ as alternative TCOs. Those tests were done to investigate the possible benefit of the a-SiO$_2$ capping layer, as a protecting layer for the encapsulated mini-modules. The investigation in this matter is still an ongoing topic, so the results shown in this work are only an initial summary that will be further analyzed in the future.

## II. Simulation details

In this work optical simulations varying the thickness of both the front TCO (ZnO:Al) and the a-SiO$_2$ AR layer were carried out to find the optimum thicknesses for the layers in the bilayer configuration. These optical simulations of the SHJ cell structure were carried out with a ray tracing model for textured surfaces using the program GenPro4 [15]. The simulated SHJ cells are taken as a multilayer structure with the n & k values determined from single layers grown on planar c-Si wafers. The n & k data were measured with an ellipsometer on the annealed, at 200°C, single layers, in order to reproduce as close as possible the properties of the layers in the real device. The program calculates the fraction of incident light absorbed in each layer. More details about the simulations can be found elsewhere [15]. In order to corroborate the simulation results, SHJ cells with the optimum ZnO:Al and a-SiO$_2$/ZnO:Al thicknesses as predicted by the simulation were processed.

## III. Experimental details

In this study two different device structures were used. 4-cm$^2$ cells on 125-μm thick (after wet processing) CZ c-Si wafer with a full-area silver rear contact were used to demonstrate the optical improvement due to the different TCOs. 244-cm$^2$ full-area bifacial cells on 160-μm thick CZ c-Si wafers were finished in glass-glass single-cell modules. The wafers were saw-damage etched and textured in KOH, and RCA cleaned prior to deposition. Since the texturing increases the total wafer surface, a factor of 1.7 will be used to calculate the deposition rate for all the layers.

The SHJ solar cells used in this work (described in Fig. 2) had an a-Si:H based i/p rear-emitter stack and a nc-Si:H FSF, all deposited in an Applied Materials (AKT1600) PECVD cluster tool operating at 13.56 MHz with a parallel electrode configuration [16]. A detailed description and analysis of the nc-Si:H layers used in this work can be found elsewhere [4, 17]. The TCO and silver layers were DC-sputtered in an in-line sputtering tool from Leybold Optics. Depositions were done through aligned shadow masks, which define 4-cm² cells, and test structures on both sides of the wafer (see Fig. 2 (b)). The ITO and ZnO:Al films were sputtered at approx. 150°C substrate temperature from a planar (97:3: In$_2$O$_3$/SnO$_2$) and a tube (1 wt. % Al$_2$O$_3$) ceramic target, respectively. At this deposition temperature, in a 110nm thick TCO layer, the mobility and sheet resistance of the ITO are around 36 cm$^2$/Vs and 90 Ω, while the ZnO:Al values are around 15 cm$^2$/Vs and 190 Ω respectively, measured on single layers grown on glass. The carrier concentration ($n_e$) of those same layers are around 2.5 and 1.8 (x10$^{20}$) cm$^{-3}$ for the ITO and the ZnO:Al respectively showing that the second material has a lower carrier concentration which might provide reduced free carrier absorption (FCA) on the solar cell devices compared to the ITO devices. When decreasing the ZnO:Al thickness to 70 nm the μ and $n_e$ stays in similar levels, to the thicker layer, but the $R_{sh}$ reaches up to 560 Ω doubling its value. Despite we use a rear emitter configuration this effect needs to be considered when reducing the thickness on solar cells.

A silver grid in a busbarless cell design with a total shading of ~3 %, with finger width ~45μm and finger pitch of 1670 μm, at the front was screen printed with a low-temperature (~200°C)

curing silver paste. The PECVD a-SiO$_2$ AR layer was finally deposited on top of the finished devices. The finished cells were measured using an AAA+ dual-source sun simulator (Wacom) under standard test conditions. External quantum efficiency (EQE) and total reflectance were measured using a dedicated test cell without grid (compare Fig. 2).

Full-area 244-cm$^2$ solar cells were processed using the same deposition steps but instead of patterning 4-cm$^2$ cells through masks during the TCO deposition only an edge exclusion mask was used on the rear side in order to prevent shunting of the cell. The metal contact of those cells was a bifacial busbarless configuration with a front grid coverage of ~4 %. Three different single-cell-modules were processed, using ITO or ZnO:Al as the TCO layer and ZnO:Al/a-SiO$_2$ as double TCO+AR layer on both sides of the device. For glass/glass single-cell-module fabrication 5 busbar cells were individually contacted with five ribbons (1.2 mm wide, 0.2 mm thick, Ulbrich Light Collecting Ribbon) glued with electrical conductive adhesive from Henkel (Hysol ECCOBOND CA3556HF) on top of the busbars. The vacuum lamination process was done at 160°C using 3.1-mm thick Ducatt solar glass at both sides of the module, with 600-µm thick acid-free polyolefin (POE) encapsulant (Mitsui TR02BA) in order to avoid any reaction with the ZnO:Al. Damp-heat tests at 85 °C and 85 % rel. humidity were done on the three different types of modules. The modules were electrically characterized after the different process steps (as processed, after 250, 500 and 1000 hours in damp-heat) using a Halm Xe Flasher and a Sensovarion HR830 electroluminescence (EL) tool.

## IV. RESULTS AND DISCUSSION

### A) Improved cells with ITO and ZnO:Al

Recent PECVD process adaptions for an improved a-Si:H passivation layer resulted in further improved cell properties yielding cell efficiencies higher than 23% for both TCOs used in this work, ITO and ZnO:Al. The bifacial ITO baseline sample obtained a 23.1 % efficiency, certified at ISFH CalTeC with a $V_{oc}$ = 741.6 mV, FF = 81.0 % and $J_{sc}$ = 38.5 mA/cm². A monofacial sample with ZnO:Al as TCO in both contacts was also certified at ISFH CalTec with an efficiency of 23.0%, $V_{oc}$ = 738.8 mV, FF = 80.3 % and $J_{sc}$ = 38.7 mA/cm². This process, however, could not yet been used in the present study.

### B) Optical Simulations Results

In order to quantify the effect of the different AR schemes optical simulations of the monofacial textured cell structure (fig. 2 (a)) were done. We varied the ZnO:Al and a-SiO$_2$ layer thicknesses in a wide range to identify the optimum layer stack. The color maps in figure 3 show the equivalent photogeneration currents under AM1-5 illumination calculated from the simulated absorption in the wafer (a) and the reflection losses

out of the cell (b) as a function of the ZnO:Al (x-axis) and the a-SiO$_2$ (y-axis) thicknesses, calculated in the range 300 - 1200 nm. We found that inserting the a-SiO$_2$ layer enhances the optical response, i.e. increases absorption in the wafer and lowers the surface reflectance, for all simulated TCO thicknesses. Especially remarkable is the improvement when the TCO thickness is lower than 55 nm. For instance, with a ZnO:Al thickness of 50 nm and a 75 nm a-SiO$_2$ the gain in simulated photogeneration current is higher than 1 mA/cm². Simulations also indicate that a further reduction of ZnO:Al thickness leads to more potential gain in current and lower reflection losses. Even though optical simulations indicate that a further thinning of the ZnO:Al thickness might be beneficial, the electrical properties of this layer need to be considered for a practical application. Higher sheet resistance ($R_{sh}$) of thin layers will cause electrical losses deteriorating the fill factor of the cells.

### C) Optical Benefits of the different AR Approaches

Aiming to find a compromise between electrical and optical gain, we selected a ZnO:Al thickness of 65 nm for the SHJ cell fabrication. After measuring optical and electrical parameters of these cells, a 55 nm thick a-SiO$_2$ layer was deposited according to our simulations to demonstrate the optical benefit of the double AR approach. A direct comparison of the experimental EQE and total reflectance (dashed lines) with the simulated absorption and the reflection profiles of the abovementioned samples are depicted in Fig. 4. As it was already observed in the simulations in Fig. 3, the double AR layer approach successfully demonstrates a gain in the absorption (Fig. 3 (a)) and lower reflectance (Fig. 3 (b)). The experimental EQE and 1- total reflection (1-R) are also plotted on each graph for comparison (dashed lines Fig. 4), demonstrating a very good match to the simulations. The $J_{sc}$ values integrated from each experimental EQE curve are given in the inset together with the simulated $J_{sc}$ values. We obtained a gain of 0.4 mA/cm² when using the improved AR double layer, both in the simulation and in the experimental results. These simulations also show a rather high parasitic absorption (1.25 mA/cm²) in the n-doped FSF layer. From previous works we know that a nc-SiO$_x$ layer can be used as FSF, together with an ITO front contact, to reduce the parasitic absorption, improve $J_{sc}$ and obtain η > 22.6 % [17, 18]. However the combination with the ZnO:Al/a-SiO$_2$ AR bilayer is still ongoing work.

The electrical parameters of the best SHJ solar cells, both for cells with 4-cm$^2$ and 244-cm$^2$ area, are summarized in Table 1. Baseline ITO samples are added as reference cells to compare the ZnO:Al with and without double AR approach. The gain in $J_{sc}$ due to a-SiO$_2$ layer incorporation is transferred to the final conversion efficiency of the cell without detrimentally affecting any other parameter, FF nor $V_{oc}$. It improved the efficiency by
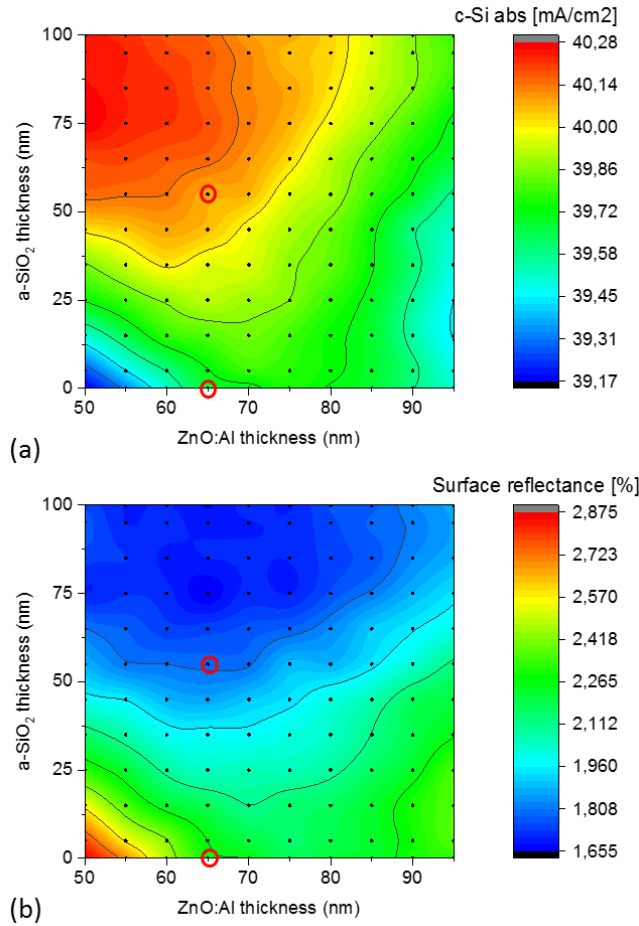
Fig. 3. Color maps of the (a) simulated equivalent current densities from light absorbed in the silicon wafer (b) and from light reflected from the surface of the simulated device in ambient air, both plotted as a function of the front ZnO:Al thickness and the a-SiO$_2$ ARC thickness. Red circles indicate the selected thicknesses used for the ZnO:Al and the a-SiO$_2$ in the experimentally realized cells.



Fig. 4. Optical simulations of the absorption in all materials and measured EQE and 1 - R curves (dashed lines) on finished cells, (a) sample with only 65 nm ZnO:Al AR, (b) sample with 55 nm a-SiO$_2$ on top of 65 nm ZnO:Al AR. The inset shows the simulated absorption in the wafer and the experimental J$_{sc}$ EQE values.

0.2 % (abs), both in the 4-cm$^2$ and the 244-cm$^2$ area cells, reaching a value as high a 23 % in the small-area cell and 21.3 % in the full-size cell.

The technology transfer from small to full-area cells is still in a rather early stage, showing a lower performance due to various effects such as the manual handling of the wafers, carriers for the different deposition processes that are still not optimized. The grid coverage of the full-size cells is also higher than the small cells, contributing to the lower J$_{sc}$ measured in those devices. Despite all these issues that need to be solved, with the full area samples developed in this work we demonstrate the optical benefit of the double AR layer also in the full area cells. In order to further analyze the full area cells, single-cell-modules were built. After the encapsulation, as expected, the current benefit of the double AR cells was

reduced to only +1 mA/cm$^2$ showing a J$_{sc}$ of 37.8 mA/cm$^2$ for the uncapped sample and a 37.9 mA/cm$^2$ for the SiO$_2$ capped sample. This lower effect of the AR approach can be attributed to the refractive index of the encapsulation material (n~1.5). The AR layers used in the modules were optically optimized for cells in ambient air. In order to obtain the highest benefit of this AR layer on module level further optimization need to be done or even alternative materials like SiN (n~2) might boost the optical benefit in module level.

Furthermore, TLM measurements on each TCO variation were done on the dedicated test structures on the front side of the devices, seen in fig. 2 (b). Thus, the R$_{sh}$, $\rho_c$ values measured correspond to the TCO to metal contact additionally helped by the conductivity of the wafer (collected in table 1). The ITO cells show better values for R$_{sh}$ and $\rho_c$ than the ZnO:Al samples

TABLE I

J-V CHARACTERISTICS OF THE BEST BUSBARLESS CELLS IN TWO DIFFERENT CELL AREAS USING THREE DIFFERENT AR METHODS

| Cell Area | Best cell (TCO thickness) | $J_{sc}$ [mA/cm$^2$] | $V_{oc}$ [mV] | FF [%] | $\eta$ [%] | TLM | |
|---|---|---|---|---|---|---|---|
| | | | | | | $R_{sh}$ [$\Omega$] | $\rho_c$ [$\Omega$cm$^2$] |
| 4-cm$^2$ | ITO ref (~75 nm) | 39.4 | 726 | 79.3 | 22.7 | 105 | 0.0043 |
| | ZnO:Al (~65 nm) | 39.6 | 730 | 78.9 | 22.8 | 140 | 0.018 |
| | ZnO:Al/a-SiO$_2$ (~65/55 nm) | 39.9 | 729 | 79.0 | 23.0 | 119 | 0.016 |
| 244-cm$^2$ | ITO ref (~75 nm) | 37.9 | 723 | 78.9 | 21.6 | - | - |
| | ZnO:Al (~65 nm) | 37.9 | 718 | 77.1 | 20.97 | - | - |
| | ZnO:Al/a-SiO$_2$ (~65/55 nm) | 38.3 | 721 | 77.2 | 21.3 | - | - |

probably due to the better conductivity and better contacts to both silver and n layer leading to a slightly better FF. Remarkable is the $R_{sh}$ improve of the ZnO:Al sample after the SiO$_2$ cap deposition which might be attributed to the TCO conductivity variation due to the hydrogen incorporation during the PECVD SiO$_2$ deposition, as seen previously by Yu *et al.* [10].

### D) Damp-heat Results

In addition to the optical improvement, the bilayer approach might have the possible benefit of protecting the underlying layers against TCO degradation, as seen by Adachi *et al.* [14]. In this section, preliminary results on the degradation of finished modules are shown. Damp-heat treatments on the single-cell-modules studied in this work were done simultaneously on the three samples, which used a 5-busbar layout to provide a good and stable contact between the grid and the glued ribbons. For details we refer to section III. The FF values of the cells after encapsulation degrade by 2% (abs.) for all samples, compared to the measurements before encapsulation. This is mostly due to the different IV contacting set-ups, namely a Pasan PCB ("grid") Touch® (30 wires) before encapsulation and conventional wiring after encapsulation. This variation is equal in all the samples not effecting our study, independently of the TCO, indicating that the SiO$_2$ is not introducing further contacting problems. Figure 5 corresponds to the experimental change (in %), relative to the initial values of each electrical parameter, from the three single-cell-modules studied in this work after 250 (dashed to the right columns), 500 hours (dashed to the left columns) and 1000 hours (filled columns). Electroluminescence (EL) images of the three samples, after encapsulation and after 1000 hours in DH, are shown in Fig. 6 to identify the origin of the degradation.

The $I_{sc}$ and $V_{oc}$ from all samples present a negligible variation, only the FF and consequently $\eta$ is clearly varying with the DH treatment time. For instance, the ITO reference sample shows even an improvement close to +1 %, which stabilizes after 250 hours in DH. We attribute this gain to a possible ribbon-wafer initial contact problem, which recovers after some time at 85°C. On the other hand the FF of the ZnO:Al sample without any cap-layer degrades ~ -1 % after 250 hours in DH and even degrades further after 500 hours in DH to ~ -2 %, but especially dramatic is the degradation after 1000 hours in DH, with a degradation higher than -7%. We assume that this degradation is due to a humidity effect on the ZnO:Al [19] inducing a loss in conductivity when the samples are under DH conditions, as observed by Greiner *et al.* [20]. ZnO:Al grows in a crystalline structure favoring a fast penetration of the water molecules in the crystal boundaries favoring degradation of the material's electrical properties. Additionally, after 1000 hours in DH it can be observed that both from EL images (fig. 6) and directly from a visual inspection on the ZnO:Al module (picture in the inset of fig. 5) a whitening of the area around the ribbons appears. This demonstrate that a possible chemical reaction might have happened on the ribbon-wafer contact probably due to the conductive glue itself. Regarding the capped sample, after 250 and 500 hours in DH a very low decrease in FF is observed, less than -1%, indicating a benefit of the a-SiO$_2$ as protective capping layer. This benefit is even more pronounced when comparing the samples after 1000 hours in DH, where the capped sample degrades less than -2% while the uncapped sample degrades more than -7% relative.

The EL image after 1000 hours in DH of the ZnO:Al sample shows a darkening on the wafer-edge around the whole perimeter, indicating that the moisture probably penetrates through the POE encapsulant at the minimodule edges degrading the ZnO:Al, as could be expected. Since the modules used in this work incorporate only single wafers, the edge effect is much higher than in a real module, where only the outer cells would be affected. In any case, this degradation could be additionally prevented by introducing edge sealing e.g. with a butyl-based solar edge tape (SET) as is common for thin-film PV modules. The EL images of the ZnO:Al/a-SiO$_2$ sample show no darkening at the edges of the module, clearly demonstrating that the a-SiO$_2$ layer acts as a protecting layer from the moisture incorporation to the ZnO:Al making the edge sealing of the modules unnecessary.
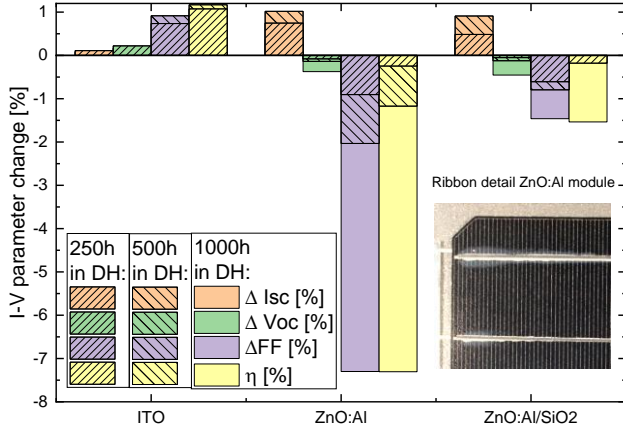
Fig. 5. I-V parameter variation after 250 (dashed to the right columns), 500 hours (dashed to the left columns) and 1000 hours (filled columns) in damp-heat treatment for the three single-cell-module analyzed in this work, as compared to the initial measurements of each cell. The picture in the inset show a detail of the ribbons on the ZnO:Al mini-module after 1000 hours in DH.
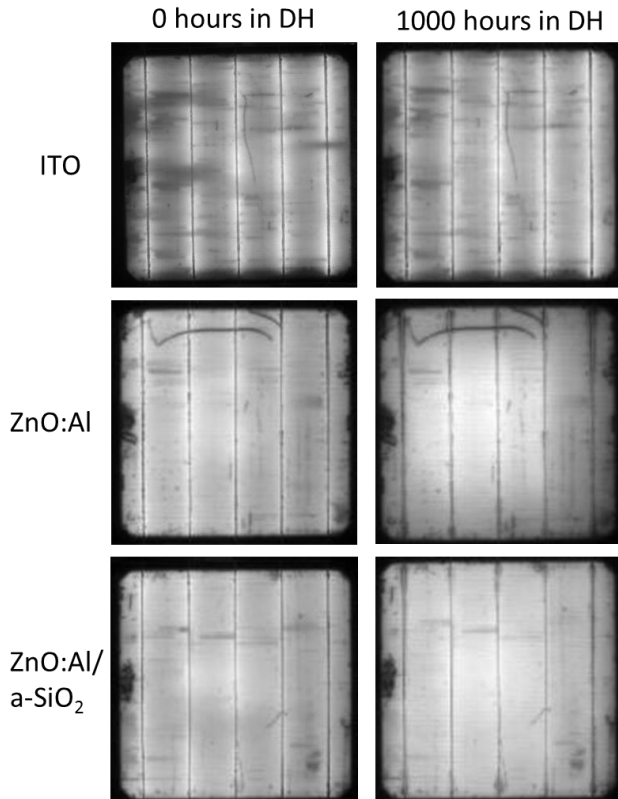


Fig. 6. Electroluminiscence (EL) images of the encapsulated single-cell-modules before the damp-heat (DH) treatment (left) and after 1000 hours in DH (right). Two different TCOs are used, ITO as a reference and ZnO:Al or ZnO:Al/SiO₂ as alternative TCO and double AR approach.

These first results show very promising results, where the modules with capped ZnO:Al degrade only -2% relative in DH. Further optimization is ongoing and it would still be possible to use even more dense or thicker capping layers, such $SiO_2$ or $SiO_xN_y$ deposited by PECVD or sputtering that would allow to obtain modules with even better performance.

## IV. CONCLUSIONS AND OUTLOOK

In this work we demonstrated that the use of ZnO:Al as a front TCO in SHJ solar cells can yield excellent light incoupling and thus improved electrical cell results compared to the ITO. Introducing the optimized double AR layer stack consisting in a 65 nm ZnO:Al and a 55 nm a-SiO₂ leads to an improvement of the short circuit current ($J_{sc}$) and efficiency ($\eta$) by +0.4 mA/cm² and +0.2 %, respectively. The best 4-cm² cell we have obtained with this bilayer approach exhibited $J_{sc}$ = 39.9 mA/cm², $V_{oc}$ = 729 mV, FF = 79 % and $\eta$ = 23 %. Furthermore, we have also observed the same optical improvement (+0.4 mA/cm²) in full-size cells, 244-cm² area, when using the double AR approach. After encapsulating equivalent cells, but with a 5-busbar layout, the current benefit of the double AR cells was reduced to only +1 mA/cm² due to the non-optimized layer thicknesses when introducing the glass and encapsulant at the front. First results of single-cell-module degradation under damp-heat (DH) conditions have been presented showing an improved stability for the ZnO:Al/a-SiO₂ sample as compared to the ZnO:Al sample without capping layer, up to 1000 hours under DH, the capped sample shows only a -2% relative efficiency degradation compared to the -7% of the uncapped module. Electroluminescence images indicate that moisture might have penetrated through the edge sealant, degrading the ZnO:Al quality of the uncapped sample, while the sample with the double AR coating show no darkening at the edges, demonstrating that the SiO₂ layer acts as a protective cover for the TCO. Further investigations on the reason for the degradation and possible alternative capping materials will be investigated in the future.

## REFERENCES

[1] D. Adachi, *et al.*, "Impact of carrier recombination on fill factor for large area heterojunction crystalline silicon solar cell with 25.1% efficiency", Applied Physics Letters 107, 233506 (2015)

[2] H. Yoshikawa *et al.*, "SHJ solar cell with interdigitated back contacts for a PV eff. over 26%", Nature Energy 2 17032 (2017)

[3] M. Bivour *et al.*, "Rear emitter silicon heterojunction solar cells: fewer restrictions on the optoelectrical properties of front side TCOs", Energy Procedia, Vol. 55, Pages 229-234, 2014.

[4] A. Morales *et al.*, "Nanocrystalline vs. amorphous n-type silicon front surface field layers in SHJ solar cells: Role of thickness and oxygen content", Proc. of EUPVSEC 2017, Amsterdam.

[5] G. Choong, *et al.*, "Transparent conductive oxides for silicon heterojunction solar cells", Proc. of EUPVSEC 2010, Valencia.

[6] A. Favier, *et al.*, "Boron-doped zinc oxide layers grown by metal-organic CVD for silicon heterojunction solar cells applications", Solar Energy Materials & Solar Cells, Vol. 95 (2011), 1057-1061.

[7] A. Dabirian, *et al.*, "Tuning the Optoelectronic Properties of ZnO:Al by Addition of Silica for Light Trapping in High-Efficiency Crystalline Si Solar Cells", Advanced Materials Interfaces, 2016, 3, 1500462.

[8] M. Balestrieri, et al., "Characterization and optimization of indium tin oxide films for heterojunction solar cells", Solar Energy Materials & Solar Cells, 95 (2011), 2390-2399.

[9] J. Geissbühler, et al., "Silicon Heterojunction Solar Cells With Copper-Plated Grid Electrodes: Status and Comparison With Silver Thick-Film Techniques ", JPV, Vol. 4, (2014), 1055-1062.

[10] J. Yu, et al., "Improved opto-electronic properties of silicon heterojunction solar cells with SiOx/Tungsten-doped indium oxide double anti-reflective coatings", Jpn. J. Appl. Phys., 56 (2017), 08MB09.

[11] R. Saive, et al., "Silicon heterojunction solar cells with effectively transparent front contacts", Sustainable Energy Fuels, 2017, 1, 593-598.

[12] D. Zhang *et al.*, "Design and fabrication of a $SiO_x$/ITO double-layer anti-reflective coating for SHJ solar cells", Solar Energy Materials & Solar Cells, Vol. 117 (2013), 132-138.

[13] S. Y Herasimenka *et al.*, "ITO/SiOx:H stacks for S solar cells", Solar Energy Materials & Solar Cells, Vol. 158 (2016), 98-101.

[14] D. Adachi, *et al.*, "Effects of $SiO_x$ barrier layer prepared by PECVD on improvement of long-term reliability and production cost for Cu-plated amorphous Si/c-Si HJ solar cells", Solar Energy Materials & Solar Cells, Vol. 163 (2017), 204-209.

[15] R. Santbergen, *et al.*, "Optical model for multilayer structures with coherent, partly coherent and incoherent layers", Optics Express, Vol. 21 (2013) p. A262-A267.

[16] O. Gabriel *et al.*, "Plasma monitoring and PECVD process control in thin film silicon-based solar cell manufacturing", EPJ Photovoltaics vol. 5, p. 55202, 2014.

[17] L. Mazzarella *et al.*, "Ultra-thin nanocrystalline n-type silicon oxide front contact layers for rear-emitter silicon heterojunction solar cells", Solar Energy Materials & Solar Cells, Vol. 179 (2018) p. 386-391.

[18] L. Mazzarella *et al.*, "Nanocrystalline n-type Silicon Oxide Front Contacts for SHJ solar cells: Photocurrent Enhancement on Planar and Textured Substrates", JPV, Vol. 8 (2017), 70-78

[19] J. Hüpkes *et al.*, "Damp heat stable doped zinc oxide films", Thin Solid Films, Vol. 555 (2014), 48-52.

[20] D. Greiner *et al.*, "Damp heat stability of Al-doped zinc oxide films on smooth and rough substrates", Thin Solid Films, Vol. 520 (2011), 1285-1290.